



MIT Open Access Articles

Multispectral imaging via luminescent down-shifting with colloidal quantum dots

The MIT Faculty has made this article openly available. **Please share** how this access benefits you. Your story matters.

Citation	Geyer, Scott M, Jennifer M. Scherer, Frank B. Jaworski, and Mounji G. Bawendi. "Multispectral imaging via luminescent down-shifting with colloidal quantum dots." <i>Optical Materials Express</i> 3, no. 8 (July 29, 2013): 1167. © 2013 OSA
As Published	http://dx.doi.org/10.1364/ome.3.001167
Publisher	Optical Society of America
Version	Final published version
Accessed	Mon Apr 25 06:26:16 EDT 2016
Citable Link	http://hdl.handle.net/1721.1/81990
Terms of Use	Article is made available in accordance with the publisher's policy and may be subject to US copyright law. Please refer to the publisher's site for terms of use.
Detailed Terms	

Multispectral imaging via luminescent down-shifting with colloidal quantum dots

Scott M Geyer,¹ Jennifer M. Scherer,¹ Frank B. Jaworski,^{2,3} and Mounqi G. Bawendi^{1,*}

¹Department of Chemistry, Massachusetts Institute of Technology, Cambridge, Massachusetts 02139, United States

²Raytheon Vision Systems, Goleta, California, United States

³frank_b_jaworski@raytheon.com

*mgb@mit.edu

Abstract: The high infrared quantum yield, continuous absorption spectrum, and band edge tunability of colloidal quantum dots (QD) has opened up new opportunities to use luminescent down shifting for multispectral imaging in the infrared. We demonstrate a QD sensitized short wavelength infrared (SWIR) camera which is capable of UV-SWIR multispectral imaging. The application of multispectral cameras for UV tagging applications is demonstrated and the extension of this technology to the mid infrared spectral region is discussed.

©2013 Optical Society of America

OCIS codes: (040.0040) Detectors; (040.3060) Infrared; (160.2540) Fluorescent and luminescent materials; (250.5590) Quantum-well, -wire and -dot devices;

References and Links

1. D. F. King, W. A. Radford, E. A. Patten, R. W. Graham, T. F. McEwan, J. G. Vodicka, R. E. Bornfreund, P. M. Goetz, G. M. Venzor, S. M. Johnson, J. E. Jensen, B. Z. Nosh, and J. A. Roth, "3rd generation 1280 x 720 FPA development status at Raytheon Vision Systems," Proc. SPIE **6206**, 62060W (2006).
2. T. Martin, R. Brubaker, P. Dixon, M.-A. Gagliardi, and T. Sudol, "640x512 InGaAs focal plane array camera for visible and SWIR imaging," Proc. SPIE **5783**, 12–20 (2005).
3. W. A. Cabanski, R. Breiter, K.-H. Mauk, W. Rode, and J. Ziegler, "Broadband and dual-color high-speed MCT MWIR modules," Proc. SPIE **4721**, 174–183 (2002).
4. J. W. Beletic, R. Blank, D. Gulbransen, D. Lee, M. Loose, E. C. Piquette, T. Sprafke, W. E. Tennant, M. Zandian, and J. Zino, "Teledyne Imaging Sensors: infrared imaging technologies for astronomy and civil space," Proc. SPIE **7021**, 70210H (2008).
5. S. M. Geyer, J. M. Scherer, N. Moloto, F. B. Jaworski, and M. G. Bawendi, "Efficient luminescent down-shifting detectors based on colloidal quantum dots for dual-band detection applications," ACS Nano **5**(7), 5566–5571 (2011).
6. S. M. Geyer, J. M. Scherer, M. G. Bawendi, and F. Jaworski, "Dual Band UV-SWIR imaging via luminescent down-shifting with colloidal quantum dots," SPIE Nano (2013).
7. G. Naletto, E. Pace, L. Placentino, and G. Tondello, "Fluorescence of metachrome in the far- and vacuum-ultraviolet spectral region," Proc. SPIE **2519**, 31–38 (1995).
8. L. Placentino, E. Pace, G. Naletto, and G. Tondello, "Performances of metachrome II as a scintillator for the far and vacuum ultraviolet spectral region," Opt. Eng. **35**(11), 3342–3347 (1996).
9. S. B. Howell, *Handbook of CCD Astronomy* (Cambridge University Press, 2006).
10. A. M. Brouwer, "Standards for photoluminescence quantum yield measurements in solution (IUPAC Technical Report)," Pure Appl. Chem. **83**(12), 2213–2228 (2011).
11. O. E. Semonin, J. C. Johnson, J. M. Luther, A. G. Midgett, A. J. Nozik, and M. C. Beard, "Absolute photoluminescence quantum yields of IR-26 dye, PbS, and PbSe quantum dots," J. Phys. Chem. Lett. **1**(16), 2445–2450 (2010).
12. B. L. Wehrenberg, C. Wang, and P. Guyot-Sionnest, "Interband and intraband optical studies of PbSe colloidal quantum dots," J. Phys. Chem. B **106**(41), 10634–10640 (2002).
13. Spectrum from IRE-640BB by Sofradir EC Inc.
14. A. B. Greytak, P. M. Allen, W. Liu, J. Zhao, E. R. Young, Z. Popovic, B. J. Walker, D. G. Nocera, and M. G. Bawendi, "Alternating layer addition approach to CdSe/CdS core/shell quantum dots with near-unity quantum yield and high on-time fractions," Chem. Sci. **3**(6), 2028–2034 (2012).
15. D. M. Reilly, D. T. Moriarty, and J. A. Maynard, "Unique properties of solar blind ultraviolet communication systems for unattended ground-sensor networks," Proc. SPIE **5611**, 244–254 (2004).
16. P. O. Anikeeva, J. E. Halpert, M. G. Bawendi, and V. Bulović, "Quantum dot light-emitting devices with electroluminescence tunable over the entire visible spectrum," Nano Lett. **9**(7), 2532–2536 (2009).

17. J. Kundu, Y. Ghosh, A. M. Dennis, H. Htoon, and J. A. Hollingsworth, "Giant nanocrystal quantum dots: stable down-conversion phosphors that exploit a large Stokes shift and efficient shell-to-core energy relaxation," *Nano Lett.* **12**(6), 3031–3037 (2012).
18. R. G. Aswathy, Y. Yoshida, T. Maekawa, and D. S. Kumar, "Near-infrared quantum dots for deep tissue imaging," *Anal. Bioanal. Chem.* **397**(4), 1417–1435 (2010).
19. J. M. Pietryga, R. D. Schaller, D. Werder, M. H. Stewart, V. I. Klimov, and J. A. Hollingsworth, "Pushing the band gap envelope: mid-infrared emitting colloidal PbSe quantum dots," *J. Am. Chem. Soc.* **126**(38), 11752–11753 (2004).
20. D. K. Harris, P. M. Allen, H.-S. Han, B. J. Walker, J. Lee, and M. G. Bawendi, "Synthesis of cadmium arsenide quantum dots luminescent in the infrared," *J. Am. Chem. Soc.* **133**(13), 4676–4679 (2011).
21. M. Yarema and M. V. Kovalenko, "Colloidal synthesis of InSb nanocrystals with controlled polymorphism using indium and antimony amides," *Chem. Mater.* **25**(9), 1788–1792 (2013).
22. S. Keuleyan, E. Lhuillier, and P. Guyot-Sionnest, "Synthesis of colloidal HgTe quantum dots for narrow mid-IR emission and detection," *J. Am. Chem. Soc.* **133**(41), 16422–16424 (2011).
23. M. Carmody, J. G. Pasko, D. Edwall, M. Daraselia, L. A. Almeida, J. Molstad, J. H. Dinan, J. K. Markunas, Y. Chen, G. Brill, and N. K. Dhar, "Long wavelength infrared, molecular beam epitaxy, HgCdTe-on-Si diode performance," *J. Electron. Mater.* **33**(6), 531–537 (2004).
24. H. Liu and P. Guyot-Sionnest, "Photoluminescence lifetime of lead selenide colloidal quantum dots," *J. Phys. Chem. C* **114**(35), 14860–14863 (2010).
25. O. Chen, J. Zhao, V. P. Chauhan, J. Cui, C. Wong, D. K. Harris, H. Wei, H.-S. Han, D. Fukumura, R. K. Jain, and M. G. Bawendi, "Compact high-quality CdSe-CdS core-shell nanocrystals with narrow emission linewidths and suppressed blinking," *Nat. Mater.* **12**(5), 445–451 (2013).
26. Y. Chen, J. Vela, H. Htoon, J. L. Casson, D. J. Werder, D. A. Bussian, V. I. Klimov, and J. A. Hollingsworth, "Giant" multishell CdSe nanocrystal quantum dots with suppressed blinking," *J. Am. Chem. Soc.* **130**(15), 5026–5027 (2008).
27. W. K. Bae, J. Joo, L. A. Padilha, J. Won, D. C. Lee, Q. Lin, W. K. Koh, H. Luo, V. I. Klimov, and J. M. Pietryga, "Highly effective surface passivation of PbSe quantum dots through reaction with molecular chlorine," *J. Am. Chem. Soc.* **134**(49), 20160–20168 (2012).
28. M. V. Kovalenko, M. Scheele, and D. V. Talapin, "Colloidal nanocrystals with molecular metal chalcogenide surface ligands," *Science* **324**(5933), 1417–1420 (2009).
29. E. Lhuillier, S. Keuleyan, P. Zolotavin, and P. Guyot-Sionnest, "Mid-infrared HgTe/As₂S₃ field effect transistors and photodetectors," *Adv. Mater.* **25**(1), 137–141 (2013).
30. M. V. Kovalenko, R. D. Schaller, D. Jarzab, M. A. Loi, and D. V. Talapin, "Inorganically functionalized PbS-CdS colloidal nanocrystals: integration into amorphous chalcogenide glass and luminescent properties," *J. Am. Chem. Soc.* **134**(5), 2457–2460 (2012).
31. S. Novak, L. Scarpantonio, J. Novak, M. D. Prè, A. Martucci, J. D. Musgraves, N. D. McClenaghan, and K. Richardson, "Incorporation of luminescent CdSe/ZnS core-shell quantum dots and PbS quantum dots into solution-derived chalcogenide glass films," *Opt. Mater. Express* **3**(6), 729–738 (2013).
32. Y. Liu, J. Tolentino, M. Gibbs, R. Ihly, C. L. Perkins, Y. Liu, N. Crawford, J. C. Hemminger, and M. Law, "PbSe quantum dot field-effect transistors with air-stable electron mobilities above 7 cm² V⁻¹ s⁻¹," *Nano Lett.* **13**(4), 1578–1587 (2013).

1. Introduction

Infrared imaging has been widely explored for civilian and military applications [1]. Of particular interest are the short wavelength infrared (SWIR, 1–2 μm), mid wavelength infrared (MWIR, 3–5 μm) and long wavelength infrared (LWIR, 8–12 μm) spectral bands, due to the high atmospheric transparency in these regions. Each of these spectral bands can provide unique capabilities; for example, the SWIR band provides improved visibility over the visible region at night [2], the MWIR band is used for tracking high temperature objects [3], and the LWIR provides thermal imaging for lower temperature objects such as humans [1]. Significant progress has been made in the development of high efficiency and high resolution imaging arrays for each of these individual bands.

Multispectral imaging uses a single camera to acquire images of an object in multiple regions of the spectrum, such as ultraviolet-visible (UV-Vis), Vis-SWIR [2], or MWIR-LWIR [1]. The ability to detect and identify objects can be greatly enhanced by analyzing the differences between the images acquired in different spectral regions, and utilizing multiple spectral bands can also overcome limitations of individual bands [1]. Although utilizing multiple single band cameras can give broad spectral response, using a different camera for each spectral region increases cost, space requirements, and power consumption. In addition, data for each spectral region is taken from a different perspective. This has motivated the development of multispectral imaging arrays that are sensitive to broad spectral regions.

Although the technology for imaging arrays for each individual spectral region is relatively highly developed, challenges remain in the fabrication of multispectral imaging arrays that operate with high efficiency across broad spectral bands. For all semiconductor based imaging cameras, the long wavelength limit is set by the band gap of the material as the photons with energy below the band gap are not absorbed. The short wavelength cut off of the detector is due to higher energy photons being absorbed in inactive regions of the detector. For example, in the case of the flip chip technology employed by many camera designs, light is absorbed by the substrate due to the backside illumination geometry [2, 4]. In Si cameras, the processing circuitry may lie above the pixel and absorb high energy photons instead of the active region.

To date, multispectral imaging has been achieved using several different techniques. For flip-chip structures where the underlying substrate absorbs the spectrum of interest, the substrate can be mechanically thinned to reduce absorption. This strategy has been employed for Vis-SWIR InGaAs detectors [2, 4]. However, this method increases cost and performance in the blue and ultraviolet regions remains poor [2, 4]. Another approach is to fabricate two junctions with different band gaps in each pixel. This has been achieved by creating a n-p-n triple layer heterojunction structure and has been employed for MWIR-LWIR two color detectors, which has the advantage of being able to select the spectral region based on the applied bias without the use of filters [1]. The main drawback is the increase in complexity and cost.

In this paper we present the use of colloidal quantum dots (QD) for luminescent down-shifting to achieve multispectral imaging [5, 6]. This method offers a simple, low cost way to expand the low wavelength spectral range of a conventional single band detector. QDs are shown to dramatically increase the sensitivity of an InGaAs SWIR imager to ultraviolet light and the use of UV-SWIR imaging for spectrally resolved tagging applications is demonstrated. The application of QDs for extending the performance of MWIR or LWIR detectors in the SWIR, Vis and UV spectral regions is modeled and discussed.

2. Luminescent down-shifting with colloidal Quantum Dots

Colloidal quantum dots are semiconductor particles with a diameter less than 50 nm that are synthesized from organo-metallic precursors using solution-phase chemistry. Figure 1(a) depicts the structure of a colloidal QD. A coating of organic ligands serves to solubilize the QDs and helps to passivate the surface. Better passivation can be achieved by growing an inorganic shell of a higher band gap material around the QD core as depicted in Fig. 1(b). Figure 1(c) shows the absorption and emission spectra for a size series of infrared emitting PbS QDs. By tuning the QD size, quantum confinement shifts the energy of the bandgap relative to the bulk bandgap of the material.

When light above the QD bandgap is absorbed, the resulting electron-hole pair rapidly relaxes to the band edge. Due to the confinement of the particle, the electron and hole cannot spatially separate, and have a high probability of recombining via the emission of a photon at the band edge. The ratio of absorbed photons to emitted photons is known as the quantum yield (QY).

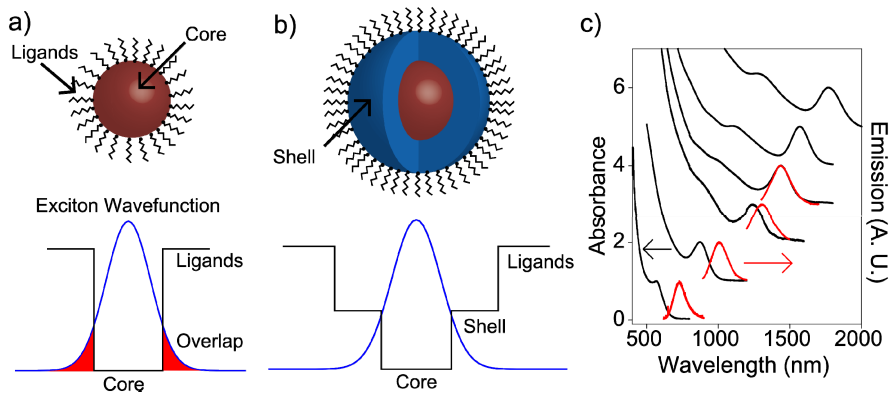


Fig. 1. (a) Cartoon of QD core surrounded by ligands and corresponding electronic structure. Note the overlap of the exciton wavefunction with the surface and ligands. (b) Core shell structure reduces overlap of the exciton with the surface. (c) Absorption (black lines) and emission (red lines) spectra of a size series of PbS QDs.

Figure 2(a) depicts the function of a QD down-shifting layer. Prior to deposition, the detector is sensitive to photons within its spectral range, but higher energy photons are absorbed outside of the active area of the detector. The QD layer is an electrically passive layer that absorbs incident photons above the band gap of the QD and re-emits the photons in the spectral range of the detector. The QDs can be embedded in a transparent polymer such as poly(methyl methacrylate) (PMMA) to improve the optical quality of the film [5]. Figure 2(b) shows the design of a QD enhanced imaging array. The bare imaging array consists of a focal plane array (FPA) that is attached to a read out integrated circuit (ROIC) via indium bumps. Following the fabrication of the imaging array, the QD layer is deposited on top of the FPA. This can be done by drop casting or spin coating to create a highly uniform layer [6].

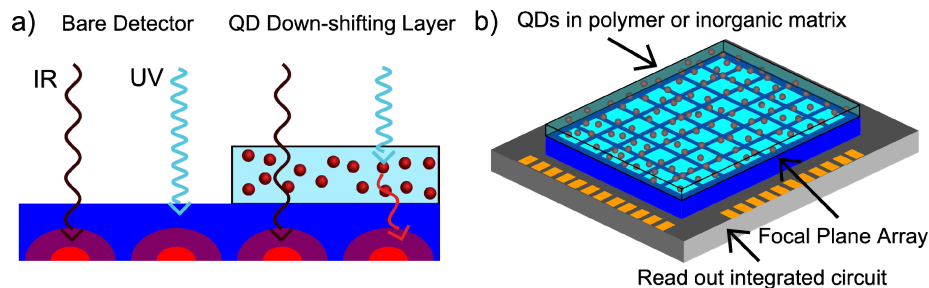


Fig. 2. (a) Cartoon of the function of the down-shifting layer. (b) Incorporation of down-shifting layer onto imaging array.

Luminescent down-shifting with organic fluorophores has been used to enhance the spectral sensitivity of Si cameras in the blue and UV regions [7–9]. However, the QY of organic dyes decreases extremely rapidly in the SWIR. Although QY values of near unity can be obtained for emission in the visible spectrum, typical QY values are below 20% by 800 nm [10] and below 1% above 1000 nm [11]. QY for QDs emitting in the SWIR region of over 80% have been reported [12], extending the application of luminescent down shifting into the infrared region.

By tuning the size, the emission wavelength can be chosen to lie along the high energy edge of a standard, single spectrum imaging array. Figures 3(a)-3(c) show the absorption and emission spectrum of PbS QDs along with the relative quantum efficiency of three different SWIR or MWIR detectors. Figures 3(a) shows the relative quantum efficiency spectrum a standard InGaAs FPA [2] and the spectra for PbS QDs emitting at 1200 nm. Figure 3(b) shows the spectrum of PbS/CdS QDs and the response of a substrate thinned InGaAs FPA

designed for Vis-SWIR dual band imaging [2]. Figure 3(c) shows the spectrum of a PbS QD emitting at 1550 nm and response curve of a HgCdTe SWIR-MWIR dual band imager [13].

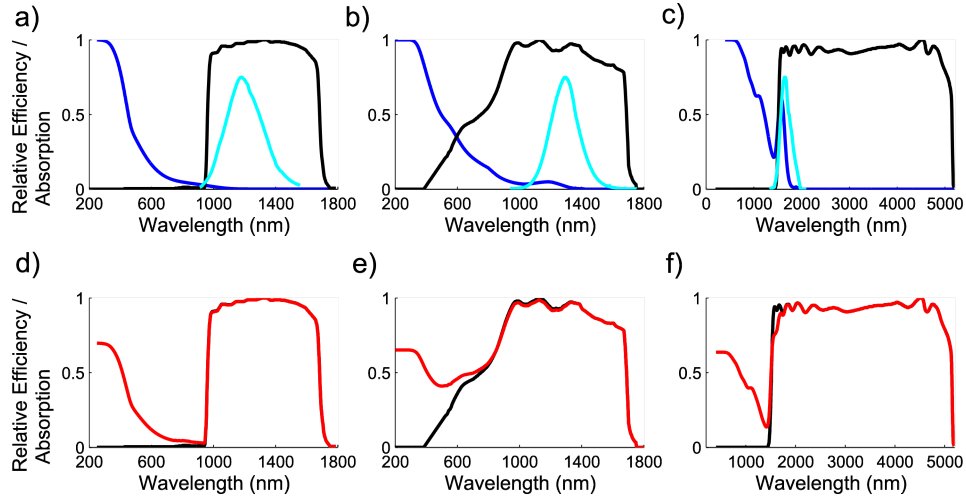


Fig. 3. (a) The relative efficiency of a bare InGaAs detector (black line) plotted with the absorption (dark blue line) and emission spectra (light blue line, arbitrary units) of PbS QDs (b) PbS/CdS QDs with a substrate thinned InGaAs imager (c) PbSe QDs with a HgCdTe MWIR imager. (e)-(f) Calculated efficiency of QD enhanced imager (red line) compared to bare imager (black line) calculated using spectra in (a)-(c) respectively.

From the absorption and emission profile of the QD and the quantum efficiency curve of the detector, the efficiency of the detector following the addition of a QD LDS layer can be modeled according to Eq. (1) [5],

$$\frac{\eta(\lambda)}{\max(\eta_{\beta})} = [1 - A(\lambda)] \frac{\eta_{\beta}(\lambda)}{\max(\eta_{\beta})} + A(\lambda) \cdot [QY \cdot CE \cdot \Theta_{em}] \quad (1)$$

In Eq. (1), $\eta_{\beta}(\lambda)/\max(\eta_{\beta})$ is the relative efficiency of the bare detector at wavelength λ , $\eta(\lambda)/\max(\eta_{\beta})$ is the calculated relative efficiency of the QD coated detector, and $A(\lambda)$ is the absorption of the QD layer. On the right side of Eq. (1), QY is the average quantum yield of the QDs, CE is the collection efficiency of emitted photons, and Θ_{em} is the overlap integral between the QD emission and the bare detector quantum efficiency.

By varying the concentration of QDs, $A(\lambda)$ can be varied such that the QDs absorb strongly in the spectral band of interest. For example, in Fig. 3(a), $A(\lambda)$ has been set such that the QDs absorb 95% of light between 250 and 400 nm. The overlap between the emission of the QDs and the bare detector, Θ_{em} , can be made near unity by tuning the QD size so that the emission overlaps with the high efficiency region of the detector as shown in Fig. 3(a). The limiting factors for performance of the down-shifting layer will therefore be the QY of the QDs and the collection efficiency, CE. For visible emitting CdSe/CdS QDs, quantum yields near 100% have been reported [14], and QYs of 80% have been obtained for SWIR emitting PbS QDs [12]. The QY of MWIR emitting QDs is discussed below. Although the QDs emit isotropically, since the index of refraction of the down-shifting layer is greater than air there is a high probability that photons emitted away from the FPA will be reflected back towards the FPA at the interface between the QD layer and air. The CE for a QD down-shifting layer with an averaged index of refraction of 1.6 is calculated to be 90% using the Fresnel equations [5].

Figures 3(d)-(f) show the calculated QE for the spectra shown in Fig. 3(a)-(c) using Eq. (1). For these calculations, a quantum yield of 80% has been used along with a collection efficiency of 90%. For the standard InGaAs FPA (Fig. 3(d)), a dramatic increase in UV sensitivity can be obtained, since the bare FPA has essentially no UV sensitivity. Even in the

case of the substrate thinned FPA that is designed for Vis performance (Fig. 3(e)), a large increase in both the Vis and UV spectral regions can be achieved to realize a UV-Vis-SWIR multispectral imager [6]. Figure 3(f) demonstrates that PbS QDs can be used to extend the spectral range of any detector that has high quantum efficiency in some portion of the SWIR region.

3. UV-SWIR Multispectral Imaging

To demonstrate the effect of the QD down-shifting layer, half of an InGaAs SWIR FPA was coated with a layer of PbS QDs in PMMA and half of the FPA was left bare. The FPA was manufactured by Raytheon Vision Systems and consists of 1280 x 1024 pixels with a 20 μm pixel pitch. The QD enhanced detector was put in a standard InGaAs camera housing and a CoastalOpt UV-Vis-IR 60 mm lens was used to reduce achromatic dispersion [6]. Figures 4(a) and 4(b) show two images from a video available online that was taken with our UV-SWIR camera at 30 frames per second. The red line separates the left half of the image which was taken with the QD coated FPA and the right half of the image which was taken with the bare FPA. In both images, the UV tag is on; however, it is not visible when imaged with the bare FPA because the UV sensitivity is so poor. When imaged with the QD coated portion it is clearly visible due to the dramatic increase in UV sensitivity. Figure 4(c) shows a single frame from a video available online which demonstrates the application of this technology for UV tagging in poor visibility situations.

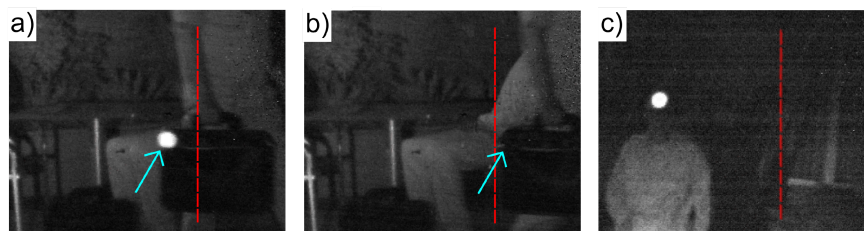


Fig. 4. (a)-(b) Scene at night. The position of a UV LED on the briefcase is indicated by the blue arrows. The portion of the FPA to the left of the dotted line is coated with QDs, while the portion to the right is bare. A dramatic change in UV sensitivity between the QD coated (a) and bare (b) FPA is observed. Video available online ([Media 1](#)). (c) Single frame from video available online demonstrating application of UV tag in low visibility situations ([Media 2](#)).

Figure 5 demonstrates the use of an ultraviolet tag in an area with large amounts of background visible and infrared sources. One challenge with using a SWIR or MWIR light emitting device (LED) as a tag or communication device is that there is a large amount of natural background in these regions. If a UV LED is used, particularly one emitting in the solar blind region between 200 and 280 nm, there is minimal background, improving the ability to detect the LED [15].

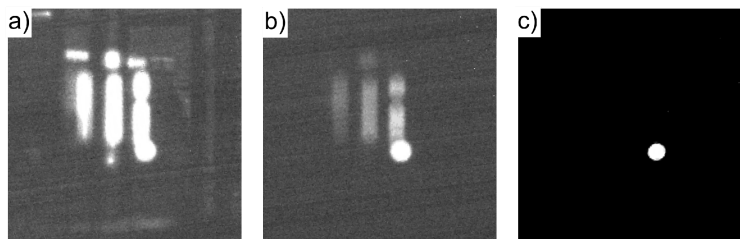


Fig. 5. Example of using multispectral imaging to identify position of tag. In image (a), a large visible and infrared background makes identification of tag difficult. In (b), a UV pass filter dramatically reduces visible and infrared response. Basic image processing can be used to generate image (c), in which the tag location is clearly identified above the background.

In Fig. 5(a), when both the UV and SWIR light is collected, identification of the tag over the background is not possible. In Fig. 5(b), a UV-pass filter (UG11 Schott glass) blocks the majority of the infrared light, revealing the location of the tag. Combining the spectra in Fig. 5(a) and 5(b), the high contrast image showing only the tag location shown in Fig. 5(c) was calculated using basic image processing according to Eq. (2),

$$I_{\text{proc}} = \left(\frac{I_{\text{UV}}}{T_{\text{UV}}} - \frac{I}{2} \right) \quad (2)$$

where T_{UV} is the average filter transmission in the UV pass band, I_{proc} is the processed image, I is the image without the UV pass filter, and I_{UV} is the filtered image. Equation (2) removes residual Vis and SWIR signal where the intensity has dropped by more than $T_{\text{UV}}/2$ when the UV pass filter is added.

The maximum frame rate of the camera will be limited by the bandwidth of the QD down-shifting layer. The bandwidth is determined by the lifetime of the QDs [5]. For visible CdSe/CdS QDs, lifetimes on the order of 10 ns are typical, which allows for approximately 15 MHz frame rates. The lifetime of PbS QDs is on the order of 1 μ s, giving a maximum frame rate of approximately 150 kHz. Figure 6 shows the response of a single pixel InGaAs detector (Hamamatsu Corporation #G8941-01) coated with PbS QDs to a 285 nm LED encoding a digital signal with a bit frequency of 10 kHz.

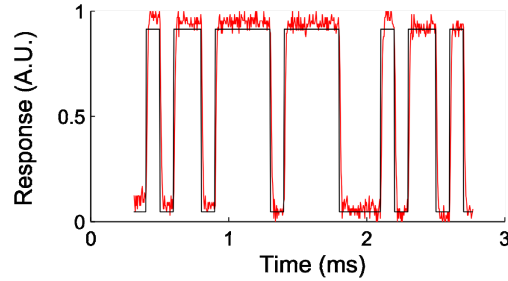


Fig. 6. Response of QD coated InGaAs detector to digitally modulated 285 nm light (red line) with corresponding digital information (black line).

The UV band is of interest for communication due to the low levels of background light in the solar blind region between 200 and 280 nm [15]. A high speed SWIR camera coated with QDs has the potential to both locate UV tags within a SWIR image and receive UV communications at rates up to 150 kHz. For example, this could be used for distinguishing between multiple UV tags within a scene.

4. Outlook for MWIR Emitting QDs

Significant effort has gone into the development and characterization of QDs that emit in the visible and SWIR spectral regions due to the commercial interest in visible LEDs [16], luminescent down shifting for white lighting [17], and biological tagging in the SWIR band [18]. Until recently, the only QD material available for MWIR emission was PbSe [19]. However, recently several syntheses have been reported for MWIR emitting QDs, including Cd₃As₂ [20], InSb [21] and HgTe [22] QDs which greatly extend the available material set for MWIR applications. Figure 7 shows the calculated effect of a QD down-shifting layer composed of HgTe QDs [22] on a LWIR detector [23].

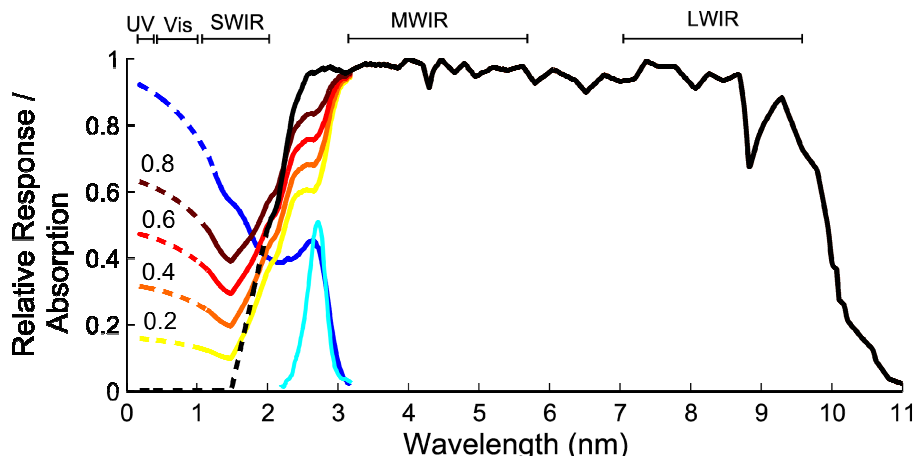


Fig. 7. Model of effect of MWIR emitting HgTe QDs [22] on the spectral response of a LWIR detector. QD absorption spectrum (dark blue line), emission spectrum (light blue line, arbitrary units) are shown along with the detector relative efficiency before addition of the QD layer (black line). The effect of the QD down-shifting layer is modeled the QY values noted on the graph above the red to yellow lines. Dashed lines are extrapolations from published data.

As Fig. 7. shows, MWIR emitting QDs show promise for ultra broad band spectral imaging. The main challenge of extending this technique into the MWIR will be to ensure a high quantum yield for the QDs. Typical synthetic methods to make quantum dots involves coating the QDs with organic ligands, as depicted in Fig. 1(a). Although these ligands serve to passivate the surface and improve the QY in the visible region, in the infrared the exciton may couple to vibrational states associated with the organic molecules leading to non-radiative recombination of the exciton [11, 24]. Therefore methods to isolate the exciton from the organic ligands are required to obtain high QY in the MWIR.

One method is to grow high quality core/shell structures that effectively to isolate the exciton from the surface. This has been achieved in the visible region with the synthesis of highly epitaxial shells that suppress blinking by isolating the exciton from the QD surface [25, 26]. Alternately, typical organic ligands may be replaced with infrared transparent fluorinated ligands [24] or with inorganic ligands [27, 28]. Another recent development is the encapsulation of QDs within an inorganic matrix [29–32]. Although a thin coating of PMMA will absorb only weakly in the MWIR region, embedding the QDs in an inorganic matrix that is completely transparent across the MWIR may improve performance and further remove the exciton from organic material.

Even if the exciton is isolated from non-radiative decay pathways associated with surface defects and organic ligands, non-radiative interband relaxation may still limit the QY of small bandgap MWIR QDs. The interband non-radiative decay rate will increase with decreasing bandgap, and may present a fundamental limit on the QY for MWIR QDs. However, MWIR and LWIR detectors are commonly cooled to reduce noise, which will decrease both the temperature of the QD coating and the non-radiative interband relaxation rate. Further experimental and theoretical work is necessary to determine the fundamental limit of the QY for MWIR emitting QDs.

5. Conclusion

We have demonstrated the use of colloidal quantum dots to extend the spectral range of an infrared detector to the ultraviolet band. The high infrared quantum yield and tunable band gap of the QDs make them uniquely suited for use as a luminescent down-shifter. The QDs can be deposited after assembly of the imaging array using low cost techniques. As synthetic techniques improve, high QY QDs emitting in the MWIR band may provide a convenient source of infrared light for a variety of applications.

Acknowledgments

This work was supported by the U.S. Army through the Institute for Soldier Nanotechnologies (W911NF-07-D-004). J. Scherer acknowledges Government support under FA9550-11-C-0028 and awarded by the Department of Defense, Air Force Office of Scientific Research, National Defense Science and Engineering Graduate (NDSEG) Fellowship, 32 CFR 168a.